

Quantum theory of a vortex line in an optical lattice

J.-P. Martikainen^{1,*} and H. T. C. Stoof^{1,†}

¹*Institute for Theoretical Physics, Utrecht University,
Leuvenlaan 4, 3584 CE Utrecht, The Netherlands*

(Dated: May 22, 2019)

Abstract

We investigate the quantum theory of a vortex line in a stack of weakly-coupled two-dimensional Bose-Einstein condensates, that is created by a one-dimensional optical lattice. We derive the dispersion relation of the Kelvin modes of the vortex line and also study the coupling between the Kelvin modes and the quadrupole modes. We solve the coupled dynamics of the vortex line and the quadrupole modes, both classically as well as quantum mechanically. The quantum mechanical solution reveals the possibility of generating nonequilibrium squeezed vortex states by strongly driving the quadrupole modes.

PACS numbers: 03.75.-b, 32.80.Pj, 03.65.-w

*Electronic address: J.P.J.Martikainen@phys.uu.nl

†Electronic address: stoof@phys.uu.nl

I. INTRODUCTION

Quantized vortices play a crucial role in understanding the stability and decay of superfluid flow. A single vortex in a Bose-Einstein condensate was first observed by Matthews *et al.* [1] and soon after that also by Madison *et al.* [2]. Since then the field has developed rapidly. The studies of a single or a few vortices [3, 4, 5, 6, 7] have more recently also been extended by experiments with Bose-Einstein condensates with a very large number of vortices [8, 9, 10, 11, 12]. Apart from some of the most recent advances, the review article by Fetter and Svidzinsky [13] provides an excellent overview of the extensive theoretical and experimental work on vortices in Bose-Einstein condensates.

While vortices are very important for understanding superfluid properties of liquids and gases, the research into Bose-Einstein condensates in optical lattices has provided an important alternative for exploring the nature of superfluidity. Bosons in an optical lattice realize the Bose-Hubbard model [14] of which the ground-state is, depending on parameters, either a superfluid or a Mott-insulator [14, 15, 16, 17, 18]. The quantum phase transition between these two phases was indeed recently observed in a beautiful experiment by Greiner *et al.* [19]. Furthermore, Bose-Einstein condensates in an optical lattice have been used to study experimentally diffraction of matter waves [20], number squeezing [21], collapses and revivals [22], superfluid dynamics [23, 24], as well as Bloch oscillations [25, 26]. There is also a number of important theoretical papers on the dynamics and instabilities of a Bose-Einstein condensate in an optical lattices [27, 28, 29, 30, 31, 32, 33].

In this paper, we study the quantum physics of a vortex line in an one-dimensional optical lattice by extending on our earlier work [34]. This problem is interesting, not only because it combines the above discussed two different approaches to the study of superfluidity in a Bose-Einstein condensate, but also because the quantum properties of the vortex are expected to be more pronounced in a system with a smaller number of particles and in lower dimensions. Furthermore, a Bose-Einstein condensate in a one-dimensional optical lattice has an intriguingly similar layered structure as the high- T_c superconductors and it also appears to be a promising way to reach the quantum Hall regime, for which we need to have about one vortex per particle [35]. Using a variational ansatz for the condensate wave function in each site of the optical potential, we derive from first principles the quantum theory of the vortex line in an one-dimensional optical lattice and obtain after linearization the dispersion relation of the Kelvin modes of the vortex line. Physically these modes correspond to a sinusoidal wiggling of the vortex line. It turns out that in an optical lattice, as compared to the system without a periodic potential, the theoretical treatment of the vortex line is considerably simplified and the dispersion relation can be obtained analytically.

Kelvin modes or kelvons were observed for the first time in a magnetically trapped Bose-Einstein condensate by Bretin *et al.* [36] and a theoretical understanding of the observed phenomena was provided by Mizushima *et al.* [37]. In this experiment, the quadrupole mode with azimuthal quantum number $m = -2$ was observed to excite the Kelvin modes. Motivated by this experiment we also use our theory to study the coupling between the kelvons and the quadrupole modes in a one-dimensional optical lattice. We find that the coupling is described by a squeezing Hamiltonian [38]. This implies that, when the vortex line is treated quantum mechanically, the quadrupole mode will generate nonequilibrium squeezed states of the vortex line. In Ref. [39] we have discussed also the spontaneous squeezing of the vortex that occurs in equilibrium if also interactions between the kelvons are taken into account. In this paper, however, we neglect these interactions and discuss

both the classical as well as the quantum dynamics of the vortex line when the vortex is driven by a strongly excited quadrupole mode. Furthermore, we discuss the dynamics of vortex squeezing and how to observe the resulting squeezed vortex states experimentally.

The paper is organized as follows. In Sec. II we present the theoretical foundations of our work. In Sec. III we discuss our variational approach and derive the Lagragian for our system. We apply the results of this section in Sec. IV, where we quantize the vortex line and find also the dispersion relation of the kelvons. In addition, we derive in Sec. IV the quantum theory of the quadrupole modes and solve their dispersion relations. In Sec. V we study the coupling between the quadrupole modes and the kelvons, and in Secs. VI and VII we explore, respectively, the classical and quantum dynamics of the vortex line that results from this coupling. In Sec VIII we discuss the nonequilibrium squeezing of the vortex line. We end with a short discussion of our results in Sec. IX.

II. ENERGY FUNCTIONAL

Our starting point is a cigar-shaped Bose-Einstein condensate trapped by the potential

$$V(\mathbf{r}) = \frac{m}{2} (\omega_r^2 r^2 + \omega_z^2 z^2), \quad (1)$$

where ω_r and ω_z are the radial and axial trapping frequencies, respectively, and m is the atomic mass. As we assume a cigar-shaped trap, we further have that $\omega_z \ll \omega_r$. The Bose-Einstein condensate also experiences an one-dimensional optical lattice

$$V_0(\mathbf{r}) = V_0 \sin^2 \left(\frac{2\pi z}{\lambda} \right), \quad (2)$$

where V_0 is the lattice depth and λ is the wave length of the laserlight. We assume that the lattice is deep enough so that it dominates over the magnetic trapping potential in the z -direction. When this is true and the number of lattice sites is very large, i.e., $\lambda \ll l_z = \sqrt{\hbar/M\omega_z}$, we can in first instance ignore the magnetic trapping potential in the z -direction.

The lattice potential splits the condensate into N_s two-dimensional condensates with a pancake shape. We take the lattice to be sufficiently deep such that its depth is larger than the chemical potential of the two-dimensional condensate. Although we are thus interested in a deep lattice, we consider here only the case that there is still full coherence across the condensate array. Specifically this means that the lattice potential should not be so deep as to induce a Mott-insulator transition. Typically the required lattice depth to reach the Mott-insulator transition in a three-dimensional lattice with a filling factor of one is of the order of $10E_r$, where E_r is the recoil energy of an atom after absorbing a photon from the laser beam. In a one-dimensional lattice the number of atoms in each lattice site is typically much larger than in a three-dimensional lattice and the transition into the insulating state requires a much deeper lattice [17]. The Mott-insulator transition in a one-dimensional optical lattice has very recently been observed [40], but also in that case the filling fraction is of the order of one.

We use trap units from now on, i.e., the unit of energy is $\hbar\omega_r$, the unit of time is $1/\omega_r$, and the unit of length is $l_r = \sqrt{\hbar/m\omega_r}$. The Gross-Pitaevskii energy functional, which describes the gas at low temperatures rotating at frequency Ω , is then

$$E [\Psi^*, \Psi] = \int d\mathbf{r} \Psi^*(\mathbf{r}) \left[-\frac{\nabla^2}{2} + \frac{1}{2} (x^2 + y^2) + \frac{V_0(\mathbf{r})}{\hbar\omega_r} + \frac{T^{2B}}{2} |\Psi(\mathbf{r})|^2 - \Omega \hat{L}_z \right] \Psi(\mathbf{r}), \quad (3)$$

where T^{2B} is the two-body T -matrix. In the above units the latter is related to the three-dimensional s -wave scattering length a through $T^{2B} = 4\pi a/l_r$. In addition,

$$\hat{L}_z = \frac{1}{i} \left(x \frac{\partial}{\partial y} - y \frac{\partial}{\partial x} \right) \quad (4)$$

is the angular momentum component in the z -direction.

For a deep lattice potential it is natural to expand the Bose-Einstein condensate wave function in terms of Wannier functions that are well localized in the sites. More precisely, we expand the Bose-Einstein condensate wave function as

$$\Psi(\mathbf{r}) = \sum_n \Phi(z - z_n) \Phi_n(x, y), \quad (5)$$

where n labels the lattice sites and $z_n = \lambda n/2l_r$ is the position of the n th site. For now we do not specify the wave functions $\Phi_n(x, y)$ of the two-dimensional condensates, but for the Wannier function in the z -direction, $\Phi(z)$, we use the ground-state wave function of the harmonic approximation to the lattice potential near the lattice minimum. This harmonic trap has the frequency

$$\omega_L = \frac{2\pi}{\lambda} \sqrt{2V_0/m} \quad (6)$$

and the wave function $\Phi(z)$ is thus given by

$$\Phi(z) = \frac{1}{\pi^{1/4} \sqrt{l_L}} \exp\left(-\frac{z^2}{2l_L^2}\right), \quad (7)$$

where $l_L = \sqrt{\hbar/m\omega_L}$.

Substituting the above ansatz into the energy functional and ignoring all but the nearest-neighbour interactions, we get the energy functional

$$\begin{aligned} E[\Phi^*, \Phi] = & \int dx dy \sum_n \left\{ \Phi_n^*(x, y) \left[-\frac{\nabla^2}{2} + \frac{1}{2} (x^2 + y^2) + \frac{U_{2D}}{2} |\Phi_n(x, y)|^2 - \Omega \hat{L}_z \right] \Phi_n(x, y) \right. \\ & \left. - J \sum_{\langle n, m \rangle} \Phi_m^*(x, y) \Phi_n(x, y) \right\}, \end{aligned} \quad (8)$$

where $\langle n, m \rangle$ indicates nearest neighbours, and

$$U_{2D} = T^{2B} \int dz |\Phi(z)|^4 = 4 \sqrt{\frac{\pi}{2}} \left(\frac{a}{l_L} \right) \quad (9)$$

is the effective two-dimensional coupling strength. Moreover, J is the strength of the Josephson coupling between neighbouring sites and we have

$$J = - \int dz \Phi^*(z) \left[-\frac{1}{2} \frac{\partial^2}{\partial z^2} + \frac{V_0(z)}{\hbar\omega_r} \right] \Phi(z + \lambda/2l_r). \quad (10)$$

With these assumptions J is a time-independent experimentally tunable parameter. Approximating the lattice potential near its maximum by an upside-down parabolic potential, we can calculate the Gaussian integral, with the result

$$J = \frac{1}{8\pi^2} \left(\frac{\omega_L}{\omega_r} \right)^2 \left(\frac{\lambda}{l_r} \right)^2 \left[\frac{\pi^2}{4} - 1 \right] e^{-(\lambda/4l_L)^2}. \quad (11)$$

The energy functional in Eq. (8) is now almost two-dimensional. The third dimension is visible only in the last term that describes the coupling between neighbouring layers. The energy is characterised by two parameters U_{2D} and J , both of which are experimentally tunable. The importance of the on-site interaction term proportional to U_{2D} can be enhanced by increasing the number of particles in the sites or by making the lattice deeper. Deepening the lattice also decreases the strength of the Josephson coupling J and makes the sites more independent. It should be noticed that while J is tunable, it is always positive. Physically this means that there is always an energetic penalty for having a phase difference between sites.

III. VARIATIONAL ANSATZ

We intend to study the coupled system of a displaced vortex line and the quadrupole modes. Therefore, a variational ansatz for the two-dimensional Bose-Einstein condensate wave function $\Phi_n(x, y, t)$ must satisfy two obvious physical requirements. Namely, the ansatz for the two-dimensional wave functions in each site must predict the vortex precession dynamics and the quadrupole mode frequencies with sufficient accuracy. The ansatz we used in an earlier publication [41] predicts the quadrupole frequencies very well from the non-interacting to the strongly-interacting limit, but unfortunately fails to predict in the strongly-interacting or Thomas-Fermi limit the correct vortex-precession dynamics. This has to do with the fact that our previous ansatz does not correctly account for the size of the vortex core in that limit. This defect is not important for the collective modes, but turns out to have serious adverse effects in predicting the vortex dynamics. Therefore, we here use the ansatz

$$\Phi_n(x, y, t) \propto \exp \left(-\frac{B_0}{2} (x^2 + y^2) - \frac{\epsilon_n(t)}{2} (x^2 - y^2) - \epsilon_{xy,n}(t)xy + i \tan^{-1} \left(\frac{y - y_n(t)}{x - x_n(t)} \right) \right), \quad (12)$$

where $(x_n(t), y_n(t))$ is the position of the vortex in the n th site and the variational parameters $\epsilon_n(t) = \epsilon'_n(t) + i\epsilon''_n(t)$ and $\epsilon_{xy,n}(t) = \epsilon'_{xy,n}(t) + i\epsilon''_{xy,n}(t)$, that describe the quadrupole and scissors modes, are complex. In addition, the wave function in each layer is normalized to N . Since our ansatz does not have a core, the average kinetic energy would diverge in this case. Therefore, we introduce a small distance cut-off ξ as an additional variational parameter. Together with the condensate size $1/\sqrt{B_0}$ this parameter will be determined by minimizing the equilibrium energy functional.

A. Equilibrium solution

In equilibrium the system has a straight vortex line in the center of the condensate. The condensate energy per particle is then given by

$$\frac{E(B_0, \xi)}{N} = \frac{1}{2B_0} + \frac{B_0}{2} + B_0 U + \frac{\xi^2}{2B_0} - \frac{B_0^2 \xi^2}{2} + \frac{1}{2} B_0 e^{B_0 \xi^2} \Gamma[0, B_0 \xi^2] - \Omega, \quad (13)$$

where

$$U = \frac{N}{\sqrt{2\pi}} \left(\frac{a}{l_r} \right) \sqrt{\frac{\omega_L}{\omega_r}}. \quad (14)$$

Furthermore, $\Gamma [a, z]$ is the incomplete gamma function. Eq. (13) is easy to minimize numerically for both ξ and B_0 , but expressions later on simplify when we note that the short distance cut-off is given, with realistic parameter values, to a very good accuracy by $\xi = \sqrt{B_0}$. After this simplification we still have to minimize the resulting transcendental equation for the remaining parameter B_0 . This is a simple numerical task that must be done only once in the beginning of the calculations.

The equilibrium solution reveals two physically obvious features. First, the Bose-Einstein condensate with the vortex is slightly bigger than the Bose-Einstein condensate without the vortex. This is due to the centrifugal potential due to the vortex velocity pattern. Second, the size of the vortex core is smaller for larger condensates. Also, it is good to keep in mind that with positive scattering lengths $0 < B_0 < 1$ and that in the Thomas-Fermi limit of large interactions we have $B_0 \ll 1$. The ansatz in Eq. (12) provides an accurate description of the system when the interaction strength U is larger than about 10. The ansatz fails for very weakly-interacting Bose-Einstein condensates, as then the energy in Eq. (13) ceases to have a minimum. In this regime our previous ansatz can however be used [41].

B. Second order expansion of the Lagrangian

As we are interested in the kelvon and quadrupole excitations we must expand the system's Lagrangian to second order in ϵ , ϵ_{xy} , x_n , and y_n . To second order there is no coupling between the quadrupole modes and the vortex displacements. Consequently, we can treat them independently. Also, as we are expanding around the equilibrium solution, we can safely ignore the zeroth and first-order contributions. The Lagrangian $L_\alpha = T_\alpha - E_\alpha$, with $\alpha = Q$ or K , for the quadrupole modes and the kelvons contain also the contributions T_α that result from the general time-derivative term in the action for the Bose-Einstein condensate given by

$$T [\Phi^*, \Phi] = \frac{i}{2} \sum_n \int dx dy \left[\Phi_n^* \dot{\Phi}_n - \Phi_n \dot{\Phi}_n^* \right], \quad (15)$$

as well the energy contribution E_α that follow from $E [\Psi^*, \Psi]$. For the quadrupole modes we obtain

$$\frac{T_Q}{N} = -\frac{1}{2B_0^2} \sum_n (\epsilon'_n \epsilon''_n + \epsilon'_{xy,n} \epsilon''_{xy,n}) \quad (16)$$

and

$$\begin{aligned} \frac{E_Q}{N} &= \sum_n \left(\frac{1}{2B_0^3} - \frac{U}{2B_0} + \frac{1}{8B_0} - \frac{\Gamma [0, B_0^2]}{4B_0} \right) (\epsilon'^2_n + \epsilon'^2_{xy,n}) + \frac{1}{2B_0} (\epsilon''^2_n + \epsilon''^2_{xy,n}) \\ &+ \left(\frac{1}{2B_0} - \frac{\Omega}{B_0^2} \right) (\epsilon'_n \epsilon''_{xy,n} - \epsilon''_n \epsilon'_{xy,n}) + \frac{J}{8B_0^2} \sum_{\langle n, m \rangle} \left[(\epsilon'_n - \epsilon'_m)^2 + (\epsilon''_n - \epsilon''_m)^2 \right. \\ &\left. + (\epsilon'_{xy,n} - \epsilon'_{xy,m})^2 + (\epsilon''_{xy,n} - \epsilon''_{xy,m})^2 \right]. \end{aligned} \quad (17)$$

For the kelvons we get, in the lowest non-vanishing order in B_0 , that

$$\frac{T_K}{N} = B_0 \sum_n (y_n \dot{x}_n - x_n \dot{y}_n) \quad (18)$$

and

$$\begin{aligned} \frac{E_K}{N} = & \frac{B_0^2}{2} \sum_n \left(1 - \Gamma [0, B_0^2] + \frac{2\Omega}{B_0^2} \right) (x_n^2 + y_n^2) \\ & + \frac{JB_0\Gamma [0, B_0^2]}{4} \sum_{\langle n, m \rangle} [(x_n - x_m)^2 + (y_n - y_m)^2]. \end{aligned} \quad (19)$$

In the absence of Josephson coupling the equations of motion for the vortex position describe the precession of a displaced vortex around the center of the condensate. With realistic interaction strengths the vortex-precession frequency predicted by Eqs. (19) and (18) is close to the result using a Thomas-Fermi wave function for the disk-shaped condensate [13].

IV. EIGENMODES OF THE SYSTEM

With the second-order expansion of the Lagrangian available, we now proceed to study the eigenmodes of the system. Our variational ansatz in Eq. (12) captures three eigenmodes, namely kelvons and two quadrupole modes with quantum numbers $m = \pm 2$. In the next two sections we solve the kelvon and the quadrupole mode dispersion relations. We deal with the nearest-neighbour Josephson coupling by transforming to momentum space in the same way as in our previous work [41]. In momentum space the terms due to the Josephson coupling are diagonal and are no more complicated than other contributions in the Lagrangian.

A. Kelvon dispersion relation

From now on we choose to interpret vortex displacements as quantum mechanical operators. This involves the important but natural approximation that the field operator $\hat{\psi}_n(x, y, t)$, which annihilates a boson in n th layer in position (x, y) at time t , can be replaced with $\Phi_n(x, y, \hat{x}_n(t), \hat{y}_n(t))$. Physically this implies that the system can be well described by a classical condensate wave function $\Phi_n(x, y)$ and that all the important quantum fluctuations are in the vortex position. Using the results in the previous section and transforming to momentum space using the convention $f_k = 1/\sqrt{N_s} \sum_n e^{-ikz_n} f_n$, we find that in momentum space the Lagrangian for the vortex line becomes

$$\begin{aligned} \frac{\hat{L}_K}{N} = & B_0 \sum_k \left(\hat{y}_k \dot{\hat{x}}_{-k} - \hat{x}_k \dot{\hat{y}}_{-k} \right) \\ & - B_0 \sum_k \left[\frac{B_0}{2} - \frac{B_0\Gamma [0, B_0^2]}{2} + \Omega + J(k)\Gamma [0, B_0^2] \right] (\hat{x}_k \hat{x}_{-k} + \hat{y}_k \hat{y}_{-k}) \end{aligned} \quad (20)$$

where $J(k) = J[1 - \cos(kd)]$. We proceed by defining the vortex positions in terms of bosonic creation and annihilation operators as $\hat{x}_k = (\hat{v}_{-k}^\dagger + \hat{v}_k)/2\sqrt{NB_0}$ and $\hat{y}_k = i(\hat{v}_{-k}^\dagger - \hat{v}_k)/2\sqrt{NB_0}$ [42]. In this manner the Lagrangian takes the desired form

$$\hat{L}_K = \sum_k \left(i\hat{v}_k^\dagger \dot{\hat{v}}_k - \omega_K(k) \hat{v}_k^\dagger \hat{v}_k \right), \quad (21)$$

where the kelvon dispersion is given by

$$\omega_K(k) = B_0/2 + \Omega + \Gamma [0, B_0^2] (2J(k) - B_0/2). \quad (22)$$

The solution at zero momentum corresponds to the precession frequency of a straight but slightly displaced vortex line.

It is important to realize that due to the Euler dynamics of the vortex, the coordinates \hat{x}_n and \hat{y}_n are canonically conjugate variables and the obey the equal-time Heisenberg commutation relation

$$[\hat{x}_n, \hat{y}_n] = \frac{i}{2NB_0}. \quad (23)$$

Our theory is valid if the vortex line precesses well within the condensate. For the straight vortex line this condition implies that the average displacement $\sqrt{\langle \hat{x}_n^2 \rangle + \langle \hat{y}_n^2 \rangle}$ should be much less than $1/\sqrt{B_0}$. This leads to a limitation for the expectation value of the number operator for the kelvons, namely,

$$\frac{1}{N_s} \sum_k \langle \hat{v}_k^\dagger \hat{v}_k \rangle \ll N. \quad (24)$$

Consequently, the total number of condensate atoms sets an upper bound for the kelvon numbers.

Our result for the kelvon dispersion relation has some interesting properties. First, the initially negative precession frequency can change sign if the momentum k of the kelvon is large enough. Moreover, the dispersion is quadratic for small momenta. Both features are due to the attractive interactions between neighbouring pancake vortices, which is harmonic for small separations. This contrasts with the behaviour of the vortex line in a three-dimensional bulk superfluid, where the kelvon dispersion relation behaves like $k^2 \ln(1/k\xi)$ and has a logarithmic dependence for small k . Third, the vortex position is “smeared” by the quantum fluctuations. In particular we have for the kelvon vacuum state that $\langle \hat{x}_n^2 \rangle = \langle \hat{y}_n^2 \rangle = 1/4NB_0$. Therefore, the quantum properties of the vortex become more important in a lattice. This is due to the reduced particle number in every site, as opposed to the total number of particles, and the spreading out of the condensate wave function as the lattice depth is increased.

B. Quadrupole mode dispersion relations

The quadrupole modes are technically somewhat more complicated than the kelvons, but their dispersion relations can be derived in a similar way. The quadrupole modes are characterized by the 4-component vector $(\hat{\epsilon}'_k, \hat{\epsilon}''_k, \hat{\epsilon}'_{xy,k}, \hat{\epsilon}''_{xy,k})$. By writing down equations of motion for all 4 variational parameters, we get a set of coupled first-order differential equations. The problem of finding the eigenmodes is then reduced to the problem of finding the eigenvectors of a 4×4 matrix. In our case this can be done analytically. We find four eigenvectors

$$\mathbf{v}_1 = \begin{pmatrix} A(k) \\ -i \\ iA(k) \\ 1 \end{pmatrix}, \quad (25)$$

$$\mathbf{v}_3 = \begin{pmatrix} -A(k) \\ i \\ iA(k) \\ 1 \end{pmatrix}, \quad (26)$$

$\mathbf{v}_2 = \mathbf{v}_1^*$, and $\mathbf{v}_4 = \mathbf{v}_3^*$. Of these solutions \mathbf{v}_1 and \mathbf{v}_2 represent the quadrupole mode with azimuthal quantum number $m = 2$, and \mathbf{v}_3 and \mathbf{v}_4 represent the quadrupole mode with azimuthal quantum number $m = -2$. The function $A(k)$ is given by

$$A(k) = \sqrt{\frac{4B_0^2 + 8B_0J(k)}{4 + 8B_0J(k) + B_0^2(1 - 4U - 2\Gamma[0, B_0^2])}}. \quad (27)$$

We can now expand any vector $(\hat{\epsilon}'_k, \hat{\epsilon}''_k, \hat{\epsilon}'_{xy,k}, \hat{\epsilon}''_{xy,k})$ into this basis of eigenvectors. Since $(\hat{\epsilon}'_k, \hat{\epsilon}''_k, \hat{\epsilon}'_{xy,k}, \hat{\epsilon}''_{xy,k})$ is a vector of hermitian operators, it is sufficient to deal only with the complex expansion amplitudes \hat{a}_1 and \hat{a}_3 of the eigenvectors \mathbf{v}_1 and \mathbf{v}_3 respectively. When we define the quadrupole creation and annihilation operators with

$$\hat{a}_1 = \sqrt{\frac{2}{NA(k)}} \frac{B_0}{4} (\hat{q}_{2,-k}^\dagger + \hat{q}_{2,k} + i\hat{q}_{2,-k}^\dagger - i\hat{q}_{2,k}) \quad (28)$$

and

$$\hat{a}_3 = \sqrt{\frac{2}{NA(k)}} \frac{B_0}{4} (\hat{q}_{-2,-k}^\dagger + \hat{q}_{-2,k} + i\hat{q}_{-2,-k}^\dagger - i\hat{q}_{-2,k}), \quad (29)$$

we ultimately find the desired Lagrangian for the quadrupole modes

$$\hat{L}_Q = \sum_{m=\pm 2} \sum_k \left(i\hat{q}_{m,k}^\dagger \dot{\hat{q}}_{m,k} - \omega_m(k) \hat{q}_{m,k}^\dagger \hat{q}_{m,k} \right), \quad (30)$$

where the quadrupole-mode frequencies are then given by

$$\begin{aligned} \omega_{\pm 2}(k) &= \frac{B_0}{A(k)} + A(k) \left(\frac{1}{B_0} + \frac{B_0}{4} - UB_0 - \frac{B_0\Gamma[0, B_0^2]}{2} \right) \\ &+ 2J(k) \left(A(k) + \frac{1}{A(k)} \right) \pm (B_0 - 2\Omega). \end{aligned} \quad (31)$$

This expression for the quadrupole frequencies generalizes our earlier result in Ref. [34] to the case of a rotating trap with $\Omega \neq 0$.

If we are to consider the quadrupole modes as a small disturbance, the distortion of the condensate due to the quadrupole modes should not be too strong. Quantitatively, we require that the energy of the quadrupole modes is much smaller than the ground-state energy of the Bose-Einstein condensate. In estimating the condensate energy we can in first instance ignore the small contribution from the vortex. In this way we obtain an upper limit for the expectation values of the quadrupole number operators as

$$\frac{1}{N_s} \sum_k \langle \hat{q}_{\pm 2,k}^\dagger \hat{q}_{\pm 2,k} \rangle \ll \sqrt{1 + 2U}. \quad (32)$$

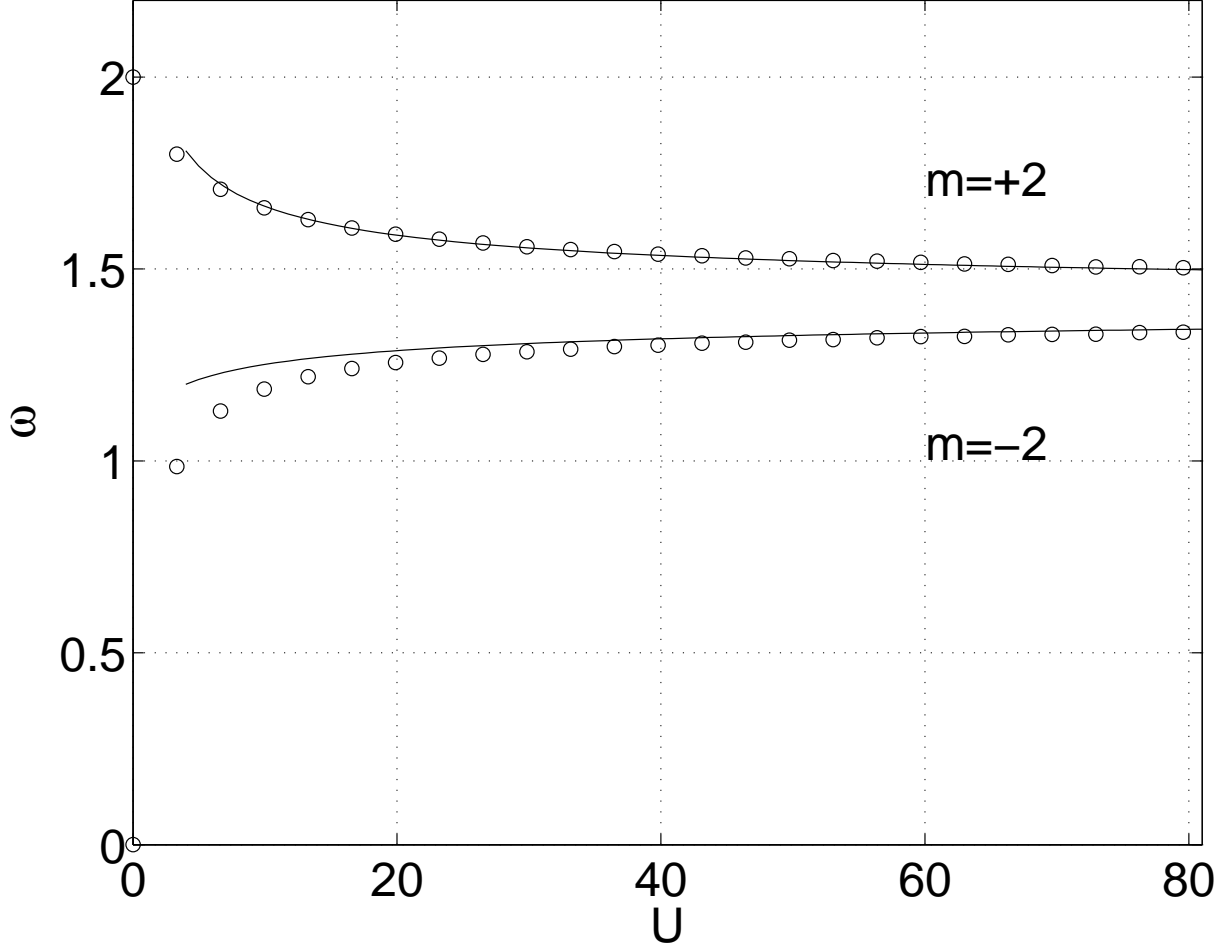


FIG. 1: Frequencies of the $m = \pm 2$ quadrupole modes for $k = 0$ and $\Omega = 0$ and as a function of interaction strength. The solid line is calculated using Eq. (31) and the open circles are calculated by solving the appropriate Bogoliubov- de Gennes equations numerically.

In Fig. 1 we compare the quadrupole dispersion relations in Eq. (31) for momentum $k = 0$ and $\Omega = 0$, with the numerical solution of the Bogoliubov-de Gennes equations for the two-dimensional Bose-Einstein condensate. As we explained earlier, our ansatz fails for very weakly-interacting Bose-Einstein condensates. Nevertheless, Fig. 1 demonstrates that Eq. (31) predicts the quadrupole-mode frequencies well within a wide range of experimentally relevant interaction strengths.

V. THE COUPLING BETWEEN KELVONS AND QUADRUPOLE MODES

In the experiment by Breten *et al.* [36] the kelvons were excited by the quadrupole mode with a quantum number $m = -2$. Therefore, we now proceed to apply our theory to investigate also the coupling between the kelvons and the quadrupole modes. To obtain coupling between the kelvons and the quadrupole modes, we must expand the Lagrangian up to third order. At third order we find important contributions from the kinetic energy, the angular momentum term, as well as from the time-derivative term. At third order there

is also a coupling between the kelvons and the quadrupole modes due to the Josephson coupling between the sites, but since we assume a small strength for this coupling we can safely ignore this. The dominant contributions are respectively given by

$$\frac{K^{(3)}}{N} = \frac{B_0 \Gamma [0, B_0^2]}{2} \sum_n [\epsilon'_n (y_n^2 - x_n^2) - 2\epsilon'_{xy,n} x_n y_n] \quad (33)$$

$$\frac{-\Omega \langle \hat{L}_z \rangle^{(3)}}{N} = \frac{\Omega}{2} \sum_n [\epsilon'_n (x_n^2 - y_n^2) + 2\epsilon'_{xy,n} x_n y_n] \quad (34)$$

and

$$\frac{T^{(3)}}{N} = \sum_n \left[-\frac{\epsilon'_n}{2} (y_n \dot{x}_n + x_n \dot{y}_n) + \frac{\epsilon'_{xy,n}}{2} (x_n \dot{x}_n - y_n \dot{y}_n) \right]. \quad (35)$$

To obtain the above relatively simple expression for $T^{(3)}$, we expanded up to first order in B_0 . Contributions at second order in B_0 depend on the details of the vortex core profile and are neglected in the following.

By using our earlier definitions for the kelvon and quadrupole creation- and annihilation operators we can express the third order contributions to the energy as

$$\begin{aligned} \hat{E}^{(3)} = & (B_0 \Gamma [0, B_0^2] - \Omega) \sum_{k,k'} \sqrt{\frac{A(k)}{8N_s}} \left[\hat{q}_{-2,k} \hat{v}_{k+k'}^\dagger \hat{v}_{-k'}^\dagger + \hat{q}_{-2,-k}^\dagger \hat{v}_{-k-k'}^\dagger \hat{v}_{k'} \right. \\ & \left. - \hat{q}_{2,k} \hat{v}_{-k-k'} \hat{v}_{k'} - \hat{q}_{2,-k}^\dagger \hat{v}_{k+k'}^\dagger \hat{v}_{-k'}^\dagger \right] \end{aligned} \quad (36)$$

and the third order contribution to the time-derivative term as

$$\begin{aligned} \hat{T}^{(3)} = & i \sum_{k,k'} \sqrt{\frac{A(k)}{8N_s}} \left[\hat{q}_{-2,k} \hat{v}_{k+k'}^\dagger \dot{\hat{v}}_{-k'}^\dagger - \hat{q}_{-2,-k}^\dagger \hat{v}_{-k-k'} \dot{\hat{v}}_{k'} \right. \\ & \left. + \hat{q}_{2,k} \hat{v}_{k'} \dot{\hat{v}}_{-k-k'} - \hat{q}_{2,-k}^\dagger \hat{v}_{k+k'}^\dagger \dot{\hat{v}}_{-k'}^\dagger \right]. \end{aligned} \quad (37)$$

Using these expression we can write down and solve the classical equation motions, but due to the time-derivatives in Eq. (37) the solution of the operator equations of motion is difficult. However, it turns out that within a wide range of experimentally realistic parameter values we can use the rotating-wave approximation to great effect and thus avoid the complication introduced by the time derivatives in Eq. (37). We, therefore, introduce the transformation $\hat{v}_k \rightarrow \hat{v}_k e^{-i\omega_K(k)t}$ and $\hat{q}_{\pm 2,k} \rightarrow \hat{q}_{\pm 2,k} e^{-i\omega_{\pm 2}(k)t}$ and ignore the remaining small time-dependent term in the transformed $\hat{T}^{(3)}$. This way we obtain the interaction picture Hamiltonians \hat{H}_m for the coupling between the kelvons and the quadrupole mode with the quantum number m as

$$\begin{aligned} \hat{H}_{-2} = & \sum_{k,k'} \sqrt{\frac{A(k')}{8N_s}} (B_0 \Gamma [0, B_0^2] - \Omega + \omega_K(k)) \left(\hat{q}_{-2,k'} \hat{v}_{k+k'}^\dagger \hat{v}_{-k}^\dagger e^{-i\delta_{-2}(k,k')t} \right. \\ & \left. + \hat{q}_{-2,-k'}^\dagger \hat{v}_{-k-k'} \hat{v}_k e^{i\delta_{-2}(k,k')t} \right) \end{aligned} \quad (38)$$

and

$$\begin{aligned}\hat{H}_2 = & \sum_{k,k'} \sqrt{\frac{A(k')}{8N_s}} \left(-B_0 \Gamma [0, B_0^2] + \Omega - \omega_K(k) \right) \left(\hat{q}_{2,k'} \hat{v}_{-k-k'} \hat{v}_k e^{-i\delta_2(k,k')t} \right. \\ & \left. + \hat{q}_{2,-k'}^\dagger \hat{v}_{k+k'}^\dagger \hat{v}_{-k}^\dagger \right) e^{-i\delta_2(k,k')t},\end{aligned}\quad (39)$$

where $\delta_{-2}(k, k') = \omega_{-2}(k') - \omega_K(k+k') - \omega_K(k)$ and $\delta_2(k, k') = -\omega_{-2}(k') - \omega_K(k+k') - \omega_K(k)$. The usual experimental preparation will typically imply that only the quadrupole mode with momentum $k' = 0$ is excited. Therefore, we from now on assume that only the $k' = 0$ quadrupole mode is present and drop the momentum index from the operator $\hat{q}_{2,-k'}$.

The coupling between the kelvons and quadrupole modes can only be important if the detunings $\delta_{\pm 2}(k, 0)$ are small. Moreover, the coupling is resonant, when the detuning vanishes. Since in the absence of rotation $\omega_K(0)$ is small and negative and $\omega_K(k)$ increases with increasing k , whereas $\omega_{\pm 2}(0)$ is positive, such a resonance is only possible between $m = -2$ quadrupole mode and the kelvons. We demonstrate this graphically in Fig. 2. This resonance condition singles out the wavelength $2\pi/k_0$ for the ensuing wiggles in the vortex line. The resonance is possible only if the kelvon frequency increases quickly enough with increasing momentum k . If, for example, the strength of the Josephson coupling J is too small, the resonance is not possible at any value of momentum. In order to have a resonant coupling between the kelvons and the quadrupole mode with $m = -2$ the approximate condition

$$J\Gamma [0, B_0^2] > \frac{1}{2\sqrt{2}} \quad (40)$$

must be satisfied. In the absence of rotation the detuning for the coupling between kelvons and $m = 2$ quadrupole modes is always large and therefore the rotating-wave approximation eliminates it.

For future convenience we define the coupling strength between the kelvons and the quadrupole mode with $m = -2$ as

$$E_c(k, k') = \sqrt{\frac{A(k')}{8N_s}} (B_0 \Gamma [0, B_0^2] - \Omega + \omega_K(k)). \quad (41)$$

In terms of this quantity the interaction picture Hamiltonian becomes

$$\hat{H}_{-2} = \sum_{k,k'} E_c(k, k') \left(\hat{q}_{-2,k'} \hat{v}_{k+k'}^\dagger \hat{v}_{-k}^\dagger e^{-i\delta_{-2}(k,k')t} + \hat{q}_{-2,-k'}^\dagger \hat{v}_{-k-k'} \hat{v}_k e^{i\delta_{-2}(k,k')t} \right). \quad (42)$$

This interaction picture Hamiltonian is similar to the Hamiltonian encountered in studies of parametric processes in quantum optics [38]. Theories describing the coupling between the atomic and molecular condensate have also a similar structure [43, 44, 45, 46, 47]. Namely, two atoms (kelvons) are combined to form a single molecule (quadrupole mode).

While the coupling between the kelvons and $m = -2$ quadrupole modes is more prevalent, the situation is slightly more involved in the rotating case. In a rotating trap the frequency of the quadrupole modes is shifted by $\mp 2\Omega$. For positive rotation frequencies this shift implies that the resonance with quadrupole modes with $m = -2$ and the kelvons is shifted to a higher value of momentum or possibly disappears altogether. On the other hand, the frequency

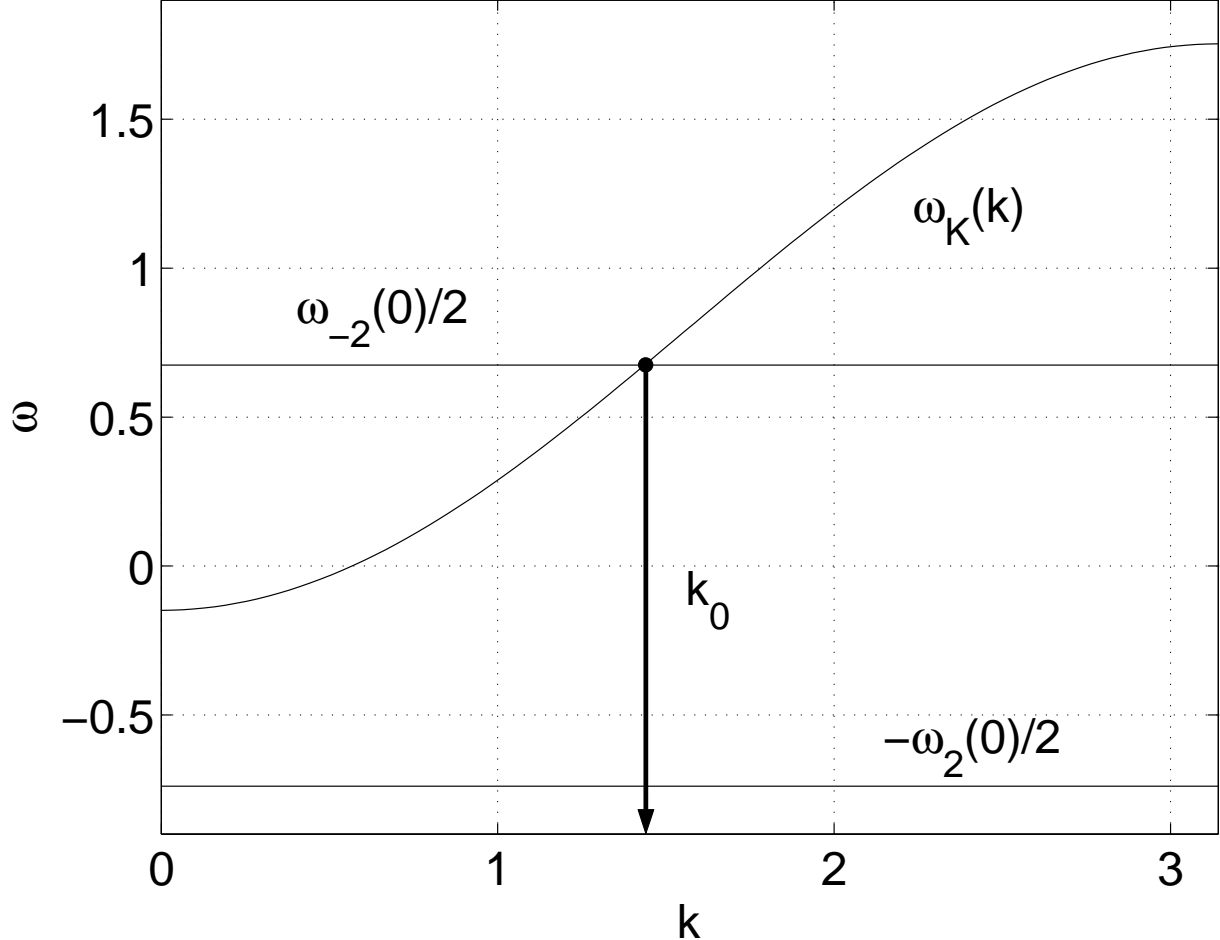


FIG. 2: Demonstration of the resonance condition for the coupling between the kelvons and the quadrupole mode with $m = -2$ when $J = 0.1$ and $U = 100$. The coupling becomes important when the kelvon frequency $\omega_K(k) = \omega_{-2}(0)/2$, i.e., when the lines cross. Since the lowest line does not cross the kelvon dispersion, the coupling between kelvons and the quadrupole mode with $m = 2$ is very weak.

of the quadrupole mode with $m = 2$ is lowered. This signifies that with sufficiently large rotation frequencies the quadrupole mode with $m = 2$ can become resonant with the kelvons. In the Thomas-Fermi limit this implies rotation frequencies larger than about $1/\sqrt{2}$. At such high rotation frequencies the dynamical instability toward the entry of additional vortices is likely to play a role [4, 48]. This unaccounted physical process makes the possibility of a strong coupling between the kelvons and $m = 2$ quadrupole modes a technical peculiarity of our variational ansatz and renders it, most likely, experimentally irrelevant.

In this paper we focus on the Bose-Einstein condensate in a one-dimensional lattice, but it is clear that the results in this section can also be applied to study an elongated condensate whose radial profile is Gaussian. The theory for the coupling between kelvons and quadrupole modes in such a system is formally similar to the one we presented here. When only quadrupole modes with $k' = 0$ are relevant, there are only two modifications. First, the kelvon dispersion relation should be replaced with the correct dispersion relation for a vortex line in an infinite cylinder with a Gaussian radial density profile. Second, the

quadrupole-mode frequencies should be replaced with the correct quadrupole frequencies for the elongated Bose-Einstein condensate. For extremely elongated condensates these frequencies have the same functional form as Eq. (31), but rather than using the interaction strength U scaled into two dimensions, we must use the correct three dimensional interaction strength.

VI. CLASSICAL DYNAMICS OF THE VORTEX LINE

In this section we apply the results in the previous sections to study the classical nonlinear dynamics of the coupled kelvons and quadrupole modes with $m = -2$. The equations of motion for the kelvons and the quadrupole mode with $m = -2$ are given by

$$i\frac{d\hat{v}_k}{dt} = E_c(k, 0)q_{-2}e^{-i\delta_{-2}(k, 0)t}\hat{v}_{-k}^\dagger, \quad (43)$$

$$i\frac{d\hat{v}_{-k}^\dagger}{dt} = -E_c(k, 0)q_{-2}^\dagger e^{i\delta_{-2}(k, 0)t}\hat{v}_k, \quad (44)$$

and

$$i\frac{dq_{-2}}{dt} = \sum_k E_c(k)\langle\hat{v}_k\hat{v}_{-k}\rangle e^{i\delta_{-2}(k, 0)t}. \quad (45)$$

In the above equations we assumed, an assumption we make throughout this paper, that the quadrupole mode is strongly excited and can thus be described with a complex number. In this section we also treat the kelvons classically, and thus the operator properties of the equations of motion will be, for the time being, ignored.

We have shown earlier how the coupling between the kelvons and the quadrupole mode with $m = -2$ becomes important at a certain value of the kelvon momentum k . From the knowledge of the kelvon and quadrupole mode dispersions we can solve the position of the resonance, but we still do not know the width of this resonance. This width is important as it influences how many kelvon modes become occupied. We obtain a simple estimate for the width of the resonance by assuming a constant quadrupole mode amplitude $q_{-2}(0)$ and by seeking exponential solutions for the kelvon amplitudes $v_k(t) \propto \exp(\Omega_{D,k}t)$. The equations of motion for the kelvon amplitudes then result in an eigenvalue problem for the characteristic frequency $\Omega_{D,k}$,

$$\hat{\Omega}_{D,k}^2 = \begin{pmatrix} (E_c(k, 0)q_{-2}(0))^2 & -\delta_{-2}(k, 0)E_c(k, 0)q_{-2}(0) \\ -\delta_{-2}(k, 0)E_c(k, 0)q_{-2}(0) & (E_c(k, 0)q_{-2}(0))^2 \end{pmatrix}. \quad (46)$$

This matrix has eigenvalues

$$\Omega_{D,k} = \pm\sqrt{E_c(k, 0)q_{-2}(0)[E_c(k, 0)q_{-2}(0) \pm |\delta_{-2}(k, 0)|]} \quad (47)$$

and therefore the Kelvin modes are dynamically unstable only when $|\delta_{-2}(k, 0)| < |E_c(k, 0)q_{-2}(0)|$. This estimate for the width of the resonance is in satisfactory agreement with the numerical solution of the nonlinear time evolution following from Eqs. (43)–(45). In addition, Eq. (47) indicates that the timescale for the onset of the instability is given by $1/|E_c(k, 0)q_{-2}(0)|$.

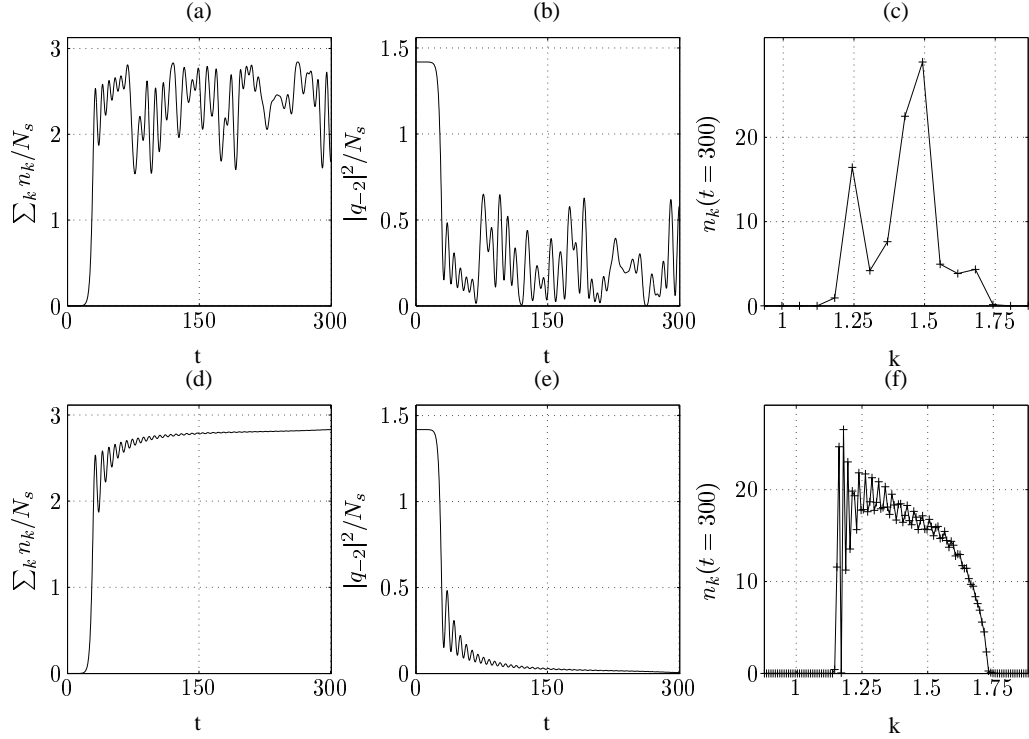


FIG. 3: (a)-(c) The time evolution of the total kelvon number per site, the quadrupole density per site, and the number distribution of kelvons in the end of the simulation, when kelvons are treated classically and $N_s = 101$. (d)-(f) These plots used the same parameters as the plots (a)-(c), except that the number of sites was larger, namely $N_s = 751$. In both sets of simulations we had initially $|q_{-2}|^2/N_s = \sqrt{1 + 2U}/10$ and a very small kelvon population to act as a seed. Also, we used $J = 0.1$ and $U = 100$. In plots (c) and (f) the + signs indicate the actual modes used in the numerical solution whereas the solid line is an interpolation between them.

The argument above was based on the assumption of having a constant quadrupole field. This assumption is bound to fail during the time evolution. When this happens, the numerical solution of the problem becomes a necessity. In Fig. 3 we show two examples of the classical time evolution of the coupled system. In this figure only the quadrupole mode is initially strongly populated. Furthermore, for numerical reasons, the kelvons have a small initial amplitude which acts as a seed for the time evolution. When the kelvons are treated quantum mechanically such a seed is not required as seen in the next section. As is clear from the figure, the quadrupole mode is strongly damped while kelvon modes are being populated. At longer times the system exhibits oscillatory behaviour, but such oscillations become weaker as the number of lattice sites is increased.

When the kelvon amplitudes are known, it is a simple matter to calculate also the dynamics of the vortex line. In Fig. 4 we show an example of the vortex line dynamics for the system solved in Fig. 3 (a)-(c). In the figure the short wavelength corresponds to the resonant mode with the momentum k_0 and the envelope with the longer wavelength is a result the width of the resonance. The fact that many kelvon modes with different momenta are occupied is also apparent from the fairly complex structure of the vortex line.

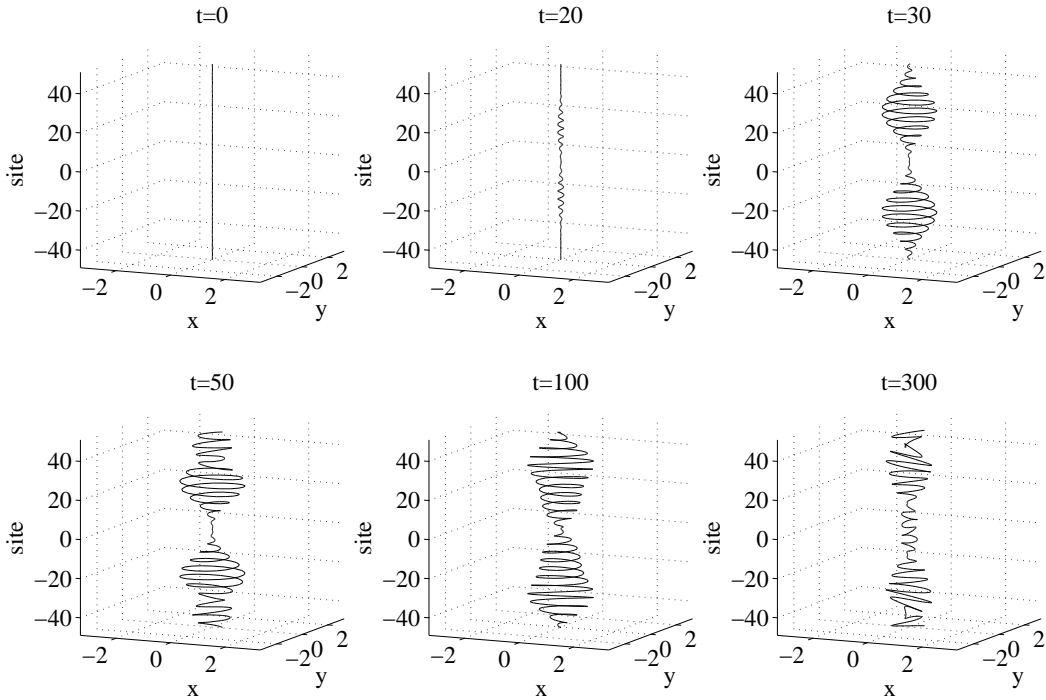


FIG. 4: Classical vortex line dynamics when $J = 0.1$, $U = 100$, and $N_s = 101$. The initial state has $|q_{-2}|^2/N_s = \sqrt{1+2U}/10$ and a very small kelvon population to act as a seed.

VII. QUANTUM DYNAMICS OF THE VORTEX LINE

In this section we discuss the quantum dynamics of the vortex line. In our numerical solution we use again a classical quadrupole mode, like in the previous section, but the kelvons are treated quantum mechanically. When the time interval Δt is short enough so that the quadrupole field $q_{-2}(t) = |q_{-2}(t)|e^{-i\phi(t)}$ can be considered as constant, we solve the Heisenberg equations of motion for the kelvons from time t to $t + \Delta t$ analytically. The result is given by

$$\hat{v}_k(t + \Delta t) = \hat{v}_k(t) \cosh(\Omega_c(t)\Delta t) - i\hat{v}_{-k}^\dagger(t) \sinh(\Omega_c(t)\Delta t) e^{-i(\phi(t) + \delta_{-2}(k,0)t)} \quad (48)$$

and

$$\hat{v}_{-k}^\dagger(t + \Delta t) = \hat{v}_{-k}^\dagger(t) \cosh(\Omega_c(t)\Delta t) + i\hat{v}_k(t) \sinh(\Omega_c(t)\Delta t) e^{i(\phi(t) + \delta_{-2}(k,0)t)}, \quad (49)$$

where $\Omega_c(t) = E_c(k, 0)|q_{-2}(t)|$. This solution enables us to update the correlation functions needed later on. In particular, we need the correlation functions $\langle \hat{v}_k \hat{v}_{-k} \rangle$ and $n_k = \langle \hat{v}_k^\dagger \hat{v}_k \rangle$ the first of which is used to update the amplitude of the quadrupole mode.

In Figs. 5 and 6 we show an example of the quantum time evolution of a system that is initially prepared in a kelvon vacuum and with a nonvanishing quadrupole-mode amplitude. It is instructive to compare Fig. 5 with its classical counterpart in Fig. 3 (d)-(e). The ambiguity of the classical initial state influences the growth rate of the classical kelvons. Therefore, detailed comparison with the quantum result cannot be easily made. Nevertheless, it is clear that in the quantum mechanical simulation the oscillatory behaviour is weaker. Fig. 6

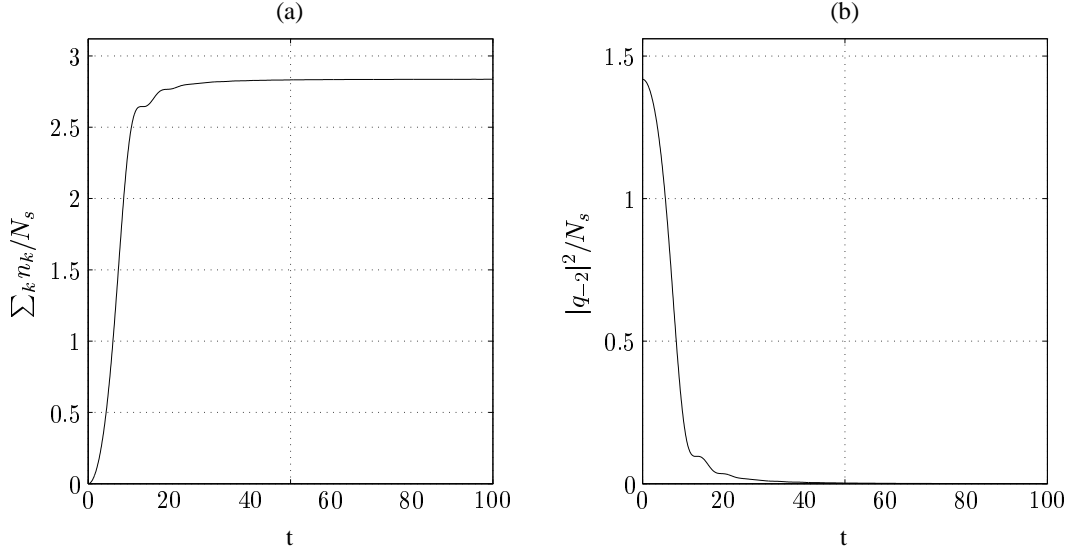


FIG. 5: (a) This plot shows the time evolution of the total average kelvon number per site for quantum mechanical kelvons. (b) This plot shows the quadrupole density per site as a function of time. In both plots we used $J = 0.1$, $U = 100$, and $N_s = 751$. Initially the system was prepared in the kelvon vacuum and with a quadrupole density $|q_{-2}|^2/N_s = \sqrt{1+2U}/10$.

FIG. 6: (Color online) This figure shows the kelvon-number distribution as a function of time when the kelvons are treated fully quantum mechanically. We used parameters $J = 0.1$, $U = 100$, and $N_s = 751$. Initially the system was prepared in the kelvon vacuum and with a quadrupole density $|q_{-2}|^2/N_s = \sqrt{1+2U}/10$.

shows the kelvon-number distribution as a function of time. After a short transient the system settles into a nearly steady state. In principle, revivals of the quadrupole field are possible, but the revival time with the number of sites we used in this simulation is longer than the length of our simulation. With fewer sites the oscillatory behaviour becomes more pronounced, in agreement with the our earlier results of the classical simulations.

A. Transition rate into kelvons using Fermi's golden rule

Fermi's golden rule

$$\Gamma_{Q \rightarrow K} = 2\pi \sum_f |\langle \Psi_f | \hat{H}_{-2} | \Psi_i \rangle|^2 \delta(E_f - E_i) \quad (50)$$

can be used to estimate the transition rate from the quadrupole mode into kelvons. In this expression $|\Psi_i\rangle$ is the initial state, $|\Psi_f\rangle$ is the final state and E_0 and E_f are their energies, respectively. In our case the initial state is a kelvon vacuum with a coherent quadrupole mode of amplitude $q_{-2}(0)$, i.e., $|\Psi_i\rangle = |q_{-2}(0), n_{k_0} = 0, n_{-k_0} = 0\rangle$. By calculating the matrix element $\langle \Psi_f | \hat{H}_{-2} | \Psi_i \rangle$ and the density of states we obtain

$$\Gamma_{Q \rightarrow K} = \frac{\pi E_c(k_0, 0)^2 |q_{-2}(0)|^2}{2J\Gamma[0, B_0^2] |\sin(k_0 d)|}, \quad (51)$$

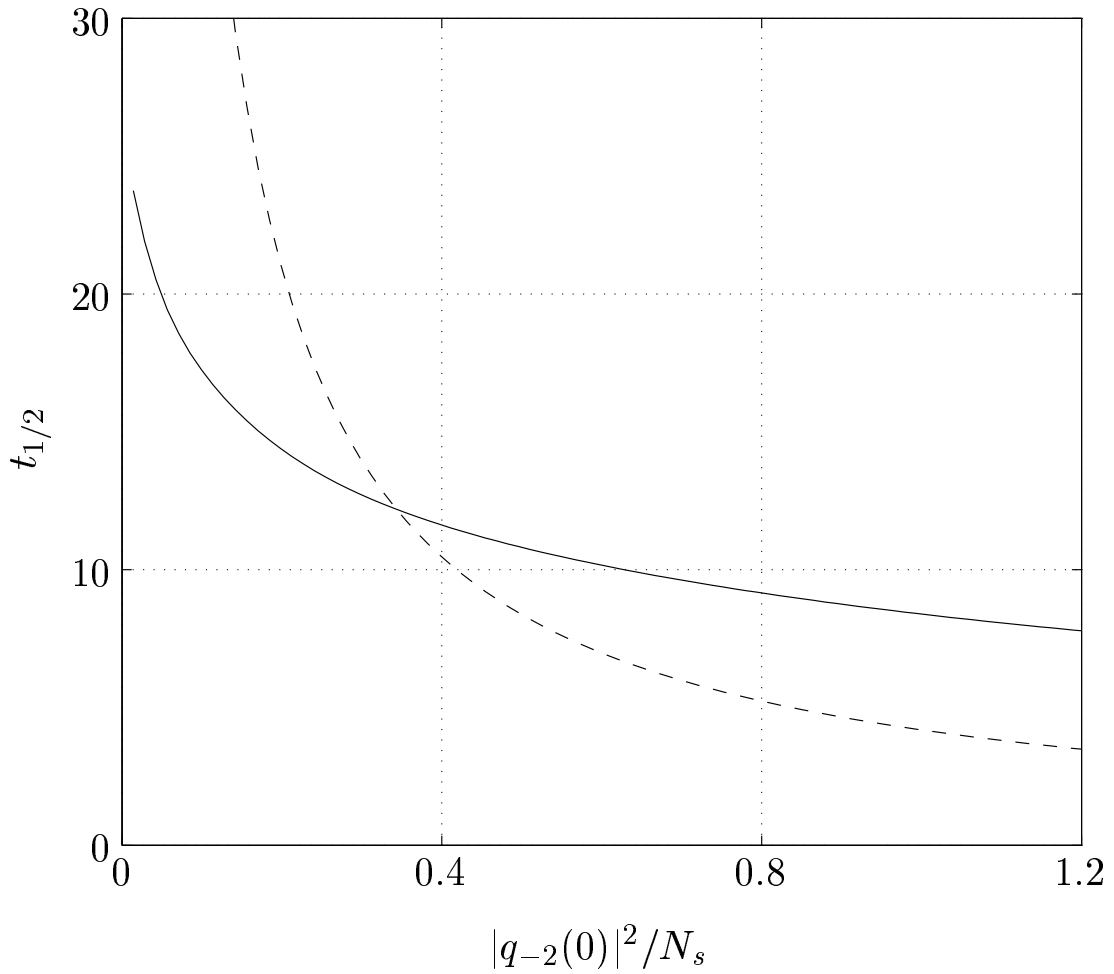


FIG. 7: This figure shows the time it takes for the quadrupole field density to halve from its initial value $|q_{-2}(0)|^2$. The solid line is based on the numerical solution of the quantum multimode problem, while the dashed line is based on Fermi's golden rule. We used parameters $J = 0.1$, $U = 100$, and $N_s = 751$.

where k_0 is the resonant value of the kelvon momentum and $d = \lambda/2$ is the lattice spacing.

Fig. 7 compares the Fermi's golden rule prediction with the numerical solution of the quantum multimode problem by presenting the half-life of the quadrupole field as a function of initial quadrupole field strength. As can be seen from this figure, Fermi's golden rule underestimates the decay rate for narrow resonances (small values of the initial quadrupole field) while overestimating the decay rate for wide resonances. The exact solution deviates from the Fermi's golden rule result, since Fermi's golden rule ignores the finite lifetime of the final states. In particular, the detunings in Eq. (45) contribute to the phase factors which determine whether the quadrupole mode is increasing or decreasing. At small times the quadrupole mode is always depleted, but at longer times the behaviour depends on the width of the resonance.

VIII. NONEQUILIBRIUM SQUEEZING

As the interaction between the quadrupole mode with $m = -2$ and the kelvons closely resembles the squeezing Hamiltonians in quantum optics, it is worth while to investigate the squeezing of the vortex in detail. This will be done in the following two subsections. We start in Sec. VIII A by discussing the squeezing when the quadrupole mode is resonantly coupled to only one Kelvin mode. Understanding this important special case enables us to explore, in Sec. VIII B, the experimentally more realistic problem of a multimode squeezing.

A. Single-mode squeezing

In the simplest case we have only one resonant kelvon mode at momentum k_0 . For simplicity we assume that initially the quadrupole mode is a real number. We can then define two quadrature operators

$$\hat{b}_1 = \frac{1}{2\sqrt{2}} \left[i\hat{v}_{-k_0} - i\hat{v}_{-k_0}^\dagger - \hat{v}_{k_0} - \hat{v}_{k_0}^\dagger \right] \quad (52)$$

and

$$\hat{b}_2 = \frac{1}{2\sqrt{2}} \left[\hat{v}_{-k_0} + i\hat{v}_{k_0} + \hat{v}_{-k_0}^\dagger - i\hat{v}_{k_0}^\dagger \right]. \quad (53)$$

These operators obey an uncertainty relation

$$\sqrt{\langle \hat{b}_1^2 \rangle} \sqrt{\langle \hat{b}_2^2 \rangle} \leq \frac{1}{4} \quad (54)$$

and their commutator is

$$[\hat{b}_1, \hat{b}_2] = \frac{i}{2}. \quad (55)$$

These operators are analogous to the squeezing operators familiar from quantum optics [38], but are somewhat counter intuitive. We gain more insight when we realize that the operators \hat{b}_i are related to the position operators $\hat{x}_k(\theta)$ and $\hat{y}_k(\theta)$ in a coordinate system rotated by an angle θ . In particular, we have $\hat{b}_1 = \sqrt{NB_0} \hat{x}_k(\theta)$ and $\hat{b}_2 = \sqrt{NB_0} \hat{y}_k(\theta)$. The rotation angle θ of the vortex position operators depends on the initial phase of the quadrupole mode, because Eqs. (52) and (53) are in principle modified if $q_{-2}(0)$ is not real. If the quadrupole mode is initially $|q_{-2}(0)|e^{i\nu_Q}$ the rotation angle is given by

$$\theta = \left(-\frac{3\pi}{2} + \nu_Q \right) / 2. \quad (56)$$

The proportionality of the quadrature operators to the vortex position operators implies that the possible squeezing of the vortex state is reflected in the corresponding deformation of the vortex-position distribution.

In Fig. 8 we show an example of the time evolution of the squares of the quadrature operators as well as the product $\sqrt{\langle \hat{b}_1^2 \rangle} \sqrt{\langle \hat{b}_2^2 \rangle}$. As can be seen from this figure, the minimum uncertainty state (the vacuum) remains a minimum uncertainty state, but can become strongly squeezed during the time evolution. In coordinate space this squeezing is reflected in the deformation of an initially circular uncertainty ellipse into an ellipse with dramatically different main axes. Furthermore, since the initial quadrupole mode amplitude was chosen as a real number, the main axes are always along the lines $y = \pm x$.

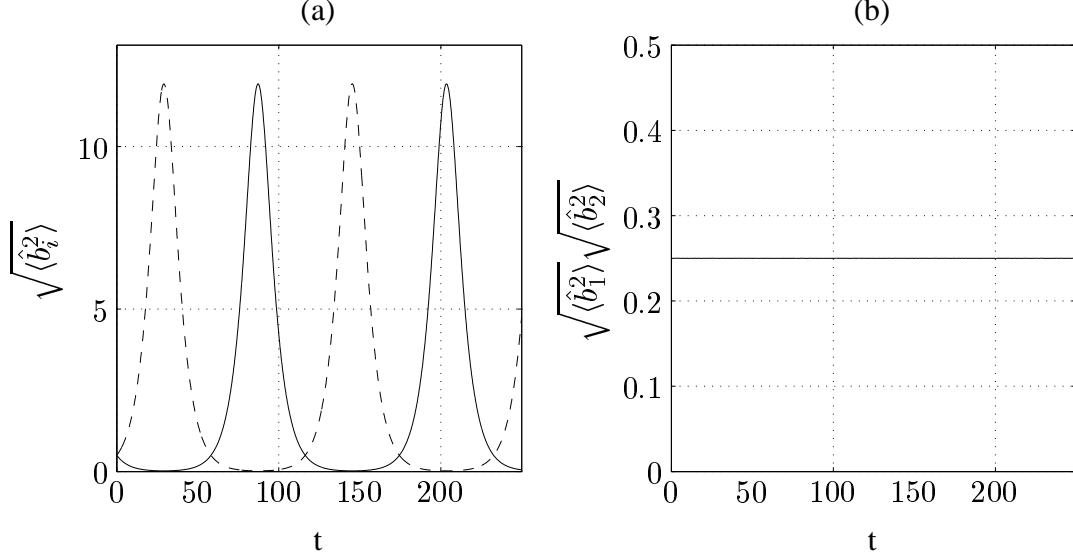


FIG. 8: (a) The time evolution of the quadrature operator uncertainty $\sqrt{\langle \hat{b}_i^2 \rangle}$. We used parameters $N_s = 100$, $N = 100$, $J = 0.1$, $U = 100$, and $|q_{-2}(0)|^2/N_s = \sqrt{1+2U}/10$. The solid line is for the operator \hat{b}_1 and the dashed line for the operator \hat{b}_2 . (b) The figure shows the time evolution for the product $\sqrt{\langle \hat{b}_1^2 \rangle} \sqrt{\langle \hat{b}_2^2 \rangle}$.

B. Multimode squeezing

The main difference between the multimode squeezing, as opposed to the resonant single-mode squeezing, is that the area of the uncertainty ellipse is no longer constant. This means that when the time evolution starts from the kelvon vacuum, the state evolves away from the minimum uncertainty state.

Generalizing our earlier results for the single-mode squeezing we define the multimode quadrature operators in terms of single-mode quadrature operators for kelvons with momentum k , $\hat{b}_{i,k}$, as

$$b_i = \frac{1}{N_s} \sum_k \hat{b}_{i,k}. \quad (57)$$

For these operators the commutator is again $[\hat{b}_1, \hat{b}_2] = \frac{i}{2}$. However, rather than embarking on this more formal road, we choose to focus on the shape of the vortex-position distribution. This distribution is measurable and provides the necessary signatures of the squeezing.

When the initial state of the vortex line is a kelvon vacuum, the fluctuations of the vortex position in a coordinate system rotated by an angle θ are given by

$$\begin{aligned} \langle \hat{x}(\theta, t)^2 \rangle &= \frac{1}{2NN_s B_0} [1 + 2n_0(t) + 2|\langle v_0(t)v_0(t) \rangle| \sin(2\theta + \phi_0(t))] \\ &+ \sum_{k \neq 0} \left(n_k(t) + \frac{1}{2} + |\langle v_k(t)v_{-k}(t) \rangle| \sin(2\theta + \phi_k(t)) \right) \end{aligned} \quad (58)$$

and

$$\begin{aligned}\langle \hat{y}(\theta, t)^2 \rangle &= \frac{1}{2NN_s B_0} [1 + 2n_0(t) - 2|\langle v_0(t)v_0(t) \rangle| \sin(2\theta + \phi_0(t)) \\ &+ \sum_{k \neq 0} \left(n_k(t) + \frac{1}{2} - |\langle v_k(t)v_{-k}(t) \rangle| \sin(2\theta + \phi_k(t)) \right)],\end{aligned}\quad (59)$$

where we defined $\langle v_k(t)v_{-k}(t) \rangle = |\langle v_k(t)v_{-k}(t) \rangle| e^{i\phi_k(t)}$. For this initial state the quantities $\langle \hat{x}(\theta, t)^2 \rangle$ and $\langle \hat{y}(\theta, t)^2 \rangle$ are independent of the site. Furthermore, their maximum and minimum with respect to the rotation angle define the lengths $\sigma_x^2(t) = \max[\langle \hat{x}(\theta, t)^2 \rangle]$ and $\sigma_y^2(t) = \min[\langle \hat{y}(\theta, t)^2 \rangle]$ of the main axes of the uncertainty ellipse as well as their directions $\theta_{max}(t)$ and $\theta_{max}(t) + \pi/2$. In terms of these quantities and in a coordinate system rotated by an angle $\theta_{max}(t)$, the uncertainty ellipse is defined by

$$\frac{x^2}{\sigma_x^2(t)} + \frac{y^2}{\sigma_y^2(t)} = 1. \quad (60)$$

The main axes of the uncertainty ellipse are in general time dependent. However, we can define the deformation parameter $\epsilon(t)$ of the uncertainty ellipse by changing the rotation angle $\theta(t)$ of the coordinate system as a function of time. In this way we define the deformation parameter as

$$\epsilon(t) = \frac{\sigma_x^2(t) - \sigma_y^2(t)}{\sigma_x^2(t) + \sigma_y^2(t)}. \quad (61)$$

In Fig. 9 we plot the time evolution of the deformation parameter with two different number of lattice sites. This figure demonstrates how the uncertainty ellipse first becomes strongly deformed and then settles into a more symmetric configuration. In the simulation with fewer number of lattice sites the strong deformation of the uncertainty ellipse revives at about $t = 60$. With larger number of lattice sites the behaviour is, at this timescale, more irreversible. In Figs. 10 and 11 we show snapshots of the uncertainty ellipses corresponding to the simulations in Fig. 9. In these figures we also indicate the main axes of the ellipses. The direction of the main axes depend on the initial phase of the quadrupole mode.

C. Experimental observation

As noted in the previous subsection the fluctuations $\langle \hat{x}(\theta)^2 \rangle$ and $\langle \hat{y}(\theta)^2 \rangle$ are independent of the site. Therefore, in each site the fluctuations of the vortex position are described by the same uncertainty ellipse and the measurement of the vortex position in each site sample the same distribution. However, the number of samples must be large enough to distinguish the squeezing from statistical fluctuations. The *in situ* imagining of the three-dimensional vortex line is difficult, but not impossible [36, 49].

In many experiments the trap potential is turned off and the system is allowed to expand. This makes the experimental imaging of the condensate as well as the vortex easier. Therefore, it is important to study how the vortex-position distribution evolves under the expansion [50, 51, 52]. We assume that only the magnetic trap is turned off and that the optical potential is left unchanged. When the small inter-site coupling is ignored, each site will expand independently in two-dimensions.

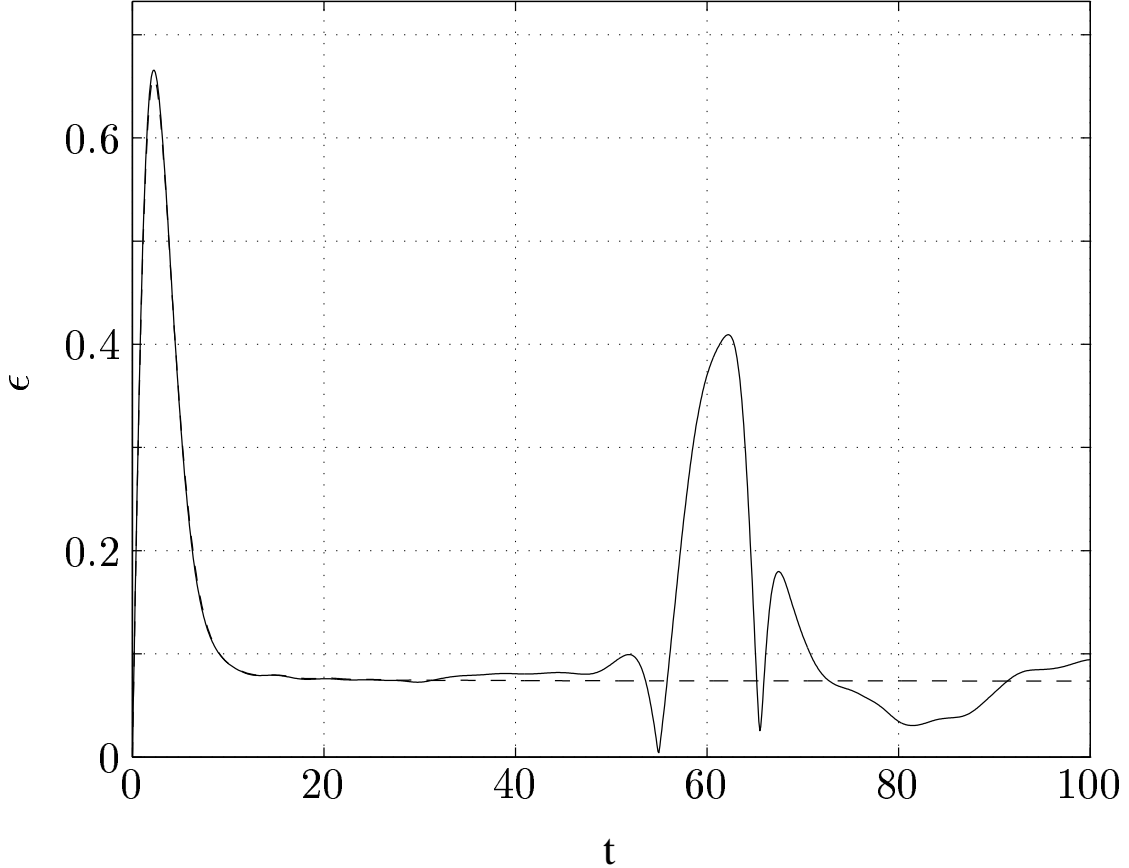


FIG. 9: This figure shows the deformation parameter of the uncertainty ellipse with two different number of lattice sites. The solid line was calculated with $N_s = 101$ and the dashed line with $N_s = 751$. In addition, we used parameters $J = 0.1$, $U = 100$, and $|q_{-2}(0)|^2/N_s = \sqrt{1 + 2U}/10$.

We study the expansion using the same variational ansatz we have used until now except that the condensate size parameter B_0 is replaced with a time-dependent complex variational parameter $B_0 \rightarrow B'_0(t) + iB''_0(t)$. The vortex core size changes as the condensate expands and we take this into account by using a time-dependent short distance cut-off

$$\xi(t) = \frac{1}{\sqrt{2UB'_0(t)}}. \quad (62)$$

This expression corresponds to the approximation that the vortex-core size is always equal to the coherence length in the center of the condensate. At $t = 0$, before the condensate expands, Eq. (62) agrees with our earlier equilibrium value for the short distance cut-off in the strongly-interacting Thomas-Fermi limit.

Up to second order in $B'_0(t)$ The equations of motion for the variational parameters are

$$\dot{x}_n(t) = C(t)x_n(t) + \omega_0(t)y_n(t), \quad (63)$$

$$\dot{y}_n(t) = C(t)y_n(t) - \omega_0(t)x_n(t), \quad (64)$$

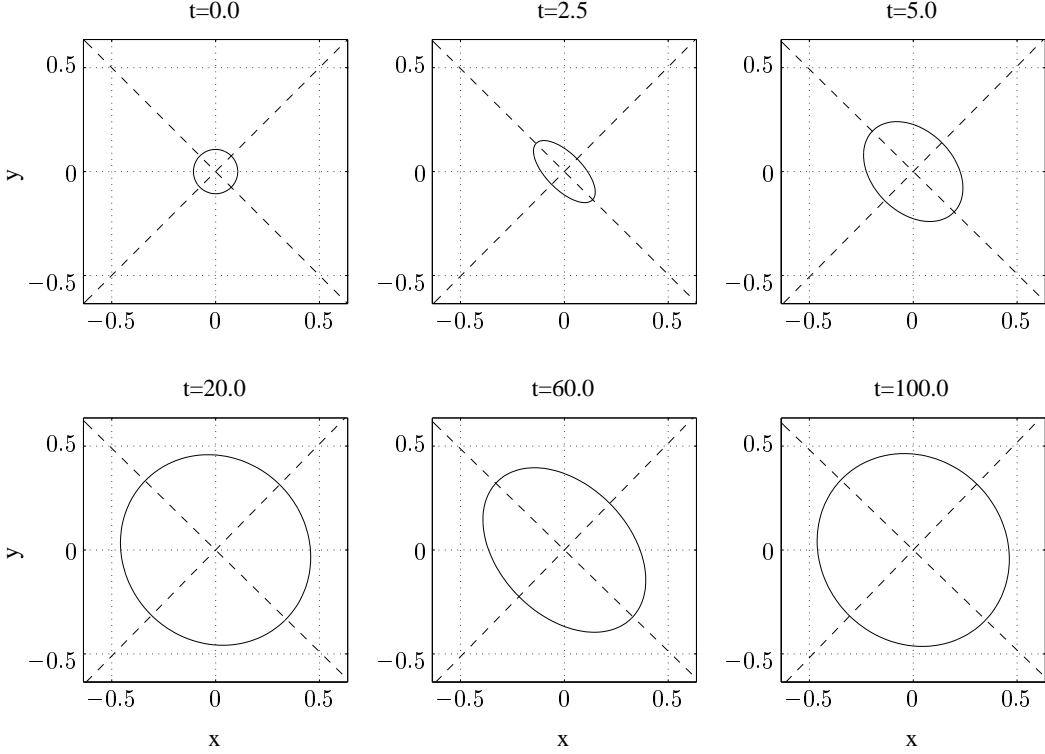


FIG. 10: This figure shows snapshots of the time evolution of the uncertainty ellipse when $N_s = 101$. In addition, we used parameters $J = 0.1$, $U = 100$, and $|q_{-2}(0)|^2/N_s = \sqrt{1 + 2U}/10$. Dashed lines indicate the directions of the main axes of the uncertainty ellipse.

$$\dot{B}'_0(t) = 2B''_0(t) \left[1 - \frac{1}{8U^2} \right] B'_0(t), \quad (65)$$

and

$$\dot{B}''_0(t) = B''_0(t)^2 \left[1 - \frac{1}{8U^2} \right] + B'_0(t)^2 \left[\gamma - 1 - \ln 2 - 2U - \ln U + \frac{1}{2U} - \frac{5}{16U^2} \right]. \quad (66)$$

To obtain the last equation we also expanded up to second order in $1/U^2$. Furthermore, $\gamma \approx 0.577216$ is the Euler-Mascheroni constant,

$$C(t) = -B''_0(t) \left[1 - \frac{1}{8U^2} \right], \quad (67)$$

and

$$\omega_0(t) = \Omega + \frac{B'_0(t)}{2} (1 - \Gamma[0, B'_0(t)^2]). \quad (68)$$

Importantly, from these equations we see that the dynamics of the expansion is independent of the vortex position. The real functions $C(t)$ and $\omega_0(t)$ depend on $B''_0(t)$ and $B'_0(t)$, respectively, but since the expansion is independent of the vortex dynamics they can be

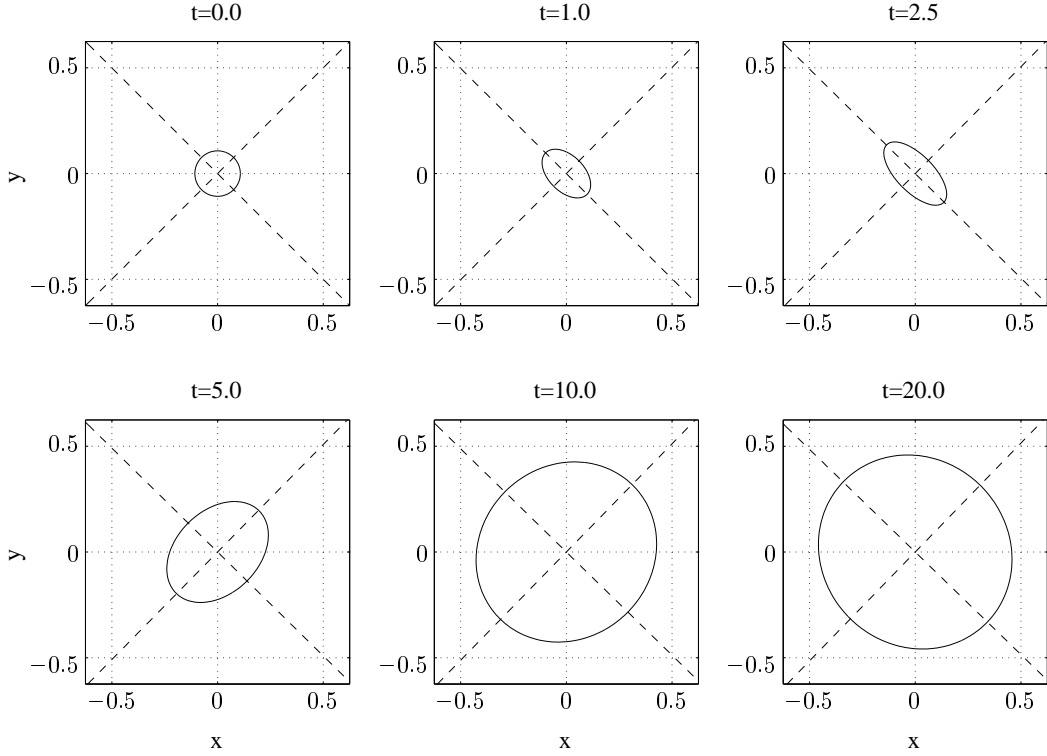


FIG. 11: This figure shows snapshots of the time evolution of the uncertainty ellipse with $N_s = 751$. In addition, we used parameters $J = 0.1$, $U = 100$, and $|q_{-2}(0)|^2/N_s = \sqrt{1 + 2U}/10$. Dashed lines indicate the directions of the main axes of the uncertainty ellipse.

considered as, in principle, given functions. The equations of motion for the vortex positions are then solved by

$$x_n(t) = \exp \left(\int_0^t C(t) dt \right) \left[x_n(0) \cos \left(\int_0^t \omega_0(t) dt \right) + y_n(0) \sin \left(\int_0^t \omega_0(t) dt \right) \right] \quad (69)$$

and

$$y_n(t) = \exp \left(\int_0^t C(t) dt \right) \left[y_n(0) \cos \left(\int_0^t \omega_0(t) dt \right) - x_n(0) \sin \left(\int_0^t \omega_0(t) dt \right) \right]. \quad (70)$$

This result shows that the vortex dynamics during the condensate expansion is a combination of precession and scaling. The precession angle and the scaling factor only depend on the dynamics of the condensate expansion and are the same irrespective of where the vortex was initially located. Therefore, a squeezed vortex distribution expands, to a very good accuracy, homologously, i.e., without changing its aspect ratio. The squeezed distribution is therefore observable even after expansion of the condensate.

In Fig. 12 we demonstrate how the expansion changes the squeezed vortex-position distribution by solving the equations of motion explicitly. This figure makes the homologous character of the expansion clearly apparent.

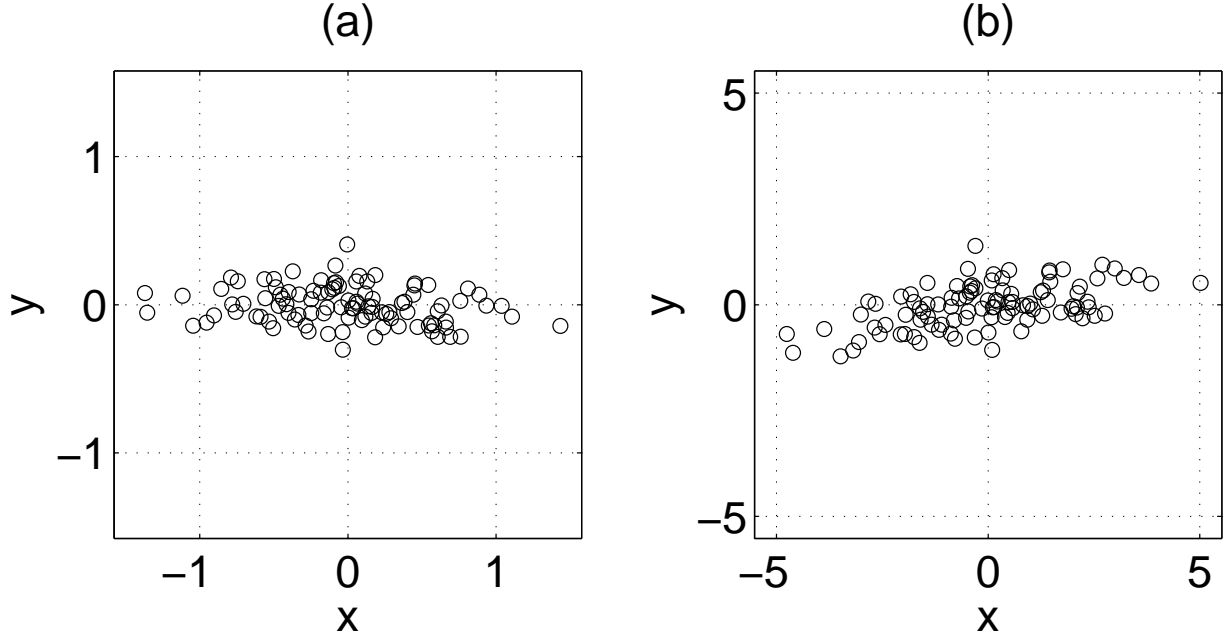


FIG. 12: This figure shows the vortex-position distribution (a) before and (b) after the expansion where condensate size increased by a factor of 3.5. We used parameters $J = 0.1$, $U = 100$, $\Omega = 0$, and $N_s = 101$. Initially vortex positions were sampled from a two-dimensional Gaussian distribution with an asymmetry of $\epsilon = 0.9$ and the product of the widths was $\sigma_x \sigma_y = B_0$.

IX. SUMMARY AND CONCLUSIONS

We derived the quantum theory of the vortex line in a one-dimensional optical lattice and obtained the dispersion relation of the Kelvin modes. Our variational approach enabled us to also include quadrupole modes into the system and study their coupling with the kelvons. The coupling turned out to be described by the squeezing Hamiltonian and we solved the dynamics of the vortex line coupled with the quadrupole mode both classically as well as quantum mechanically. Furthermore, we found that the vortex line can indeed be squeezed in this system if we drive the quadrupole modes sufficiently strongly. We also discussed some of the expected experimental signatures.

Our theory can be applied to a variety of new problems. For example, exploring the properties of the vortex line at finite temperatures is possible by adapting the theory we have used in this paper [39]. Also, the interplay between the superfluid Mott-insulator transition, the quantum melting of a vortex lattice, and the quantum-Hall regime in an optical lattice is a very interesting topic for further research.

Acknowledgments

We thank Randy Hulet for suggesting to us to consider also the vortex-position distribution after expansion. This work is supported by the Stichting voor Fundamenteel Onderzoek der Materie (FOM) and by the Nederlandse Organisatie voor Wetenschappelijk Onderzoek

(NWO).

- [1] M. R. Matthews, B. P. Anderson, P. C. Haljan, D. S. Hall, C. E. Wieman, and E. A. Cornell, Phys. Rev. Lett. **83**, 2498 (1999).
- [2] K. Madison, F. Chevy, W. Wohlleben, and J. Dalibard, Phys. Rev. Lett. **84**, 806 (2000).
- [3] E. Hodby, O. M. Maragó, G. Hechenblaikner, and C. J. Foot, Phys. Rev. Lett. **86**, 2196 (2001).
- [4] E. Hodby, G. Hechenblaikner, S. A. Hopkins, O. M. Maragó, and C. J. Foot, Phys. Rev. Lett. **88**, 010405 (2002).
- [5] P. Rosenbusch, V. Bretin, and J. Dalibard, Phys. Rev. Lett. **88**, 200403 (2002).
- [6] A. E. Leanhardt, A. Görlitz, A. P. Chikkatur, D. Kielpinski, Y. Shin, D. E. Pritchard, and W. Ketterle, Phys. Rev. Lett. **89**, 190403 (2002).
- [7] A. E. Leanhardt, Y. Shin, D. Kielpinski, D. E. Pritchard, and W. Ketterle, Phys. Rev. Lett. **90**, 140403 (2003).
- [8] J. R. Abo-Shaeer, C. Raman, J. M. Vogels, and W. Ketterle, Science **292**, 476 (2001).
- [9] J. R. Abo-Shaeer, C. Raman, and W. Ketterle, Phys. Rev. Lett. **88**, 070409 (2002).
- [10] P. Engels, I. Coddington, P. C. Haljan, and E. A. Cornell, Phys. Rev. Lett. **89**, 100403 (2002).
- [11] P. Engels, I. Coddington, P. C. Haljan, V. Schweikhard, and E. A. Cornell, Phys. Rev. Lett. **90**, 170405 (2003).
- [12] I. Coddington, P. Engels, V. Schweikhard, and E. A. Cornell, Phys. Rev. Lett. **91**, 100402 (2003).
- [13] A. L. Fetter and A. A. Svidzinsky, J. Phys.:Condens. Matter **13**, R135 (2001), and references therein.
- [14] D. Jaksch, C. Bruder, J. Cirac, C. W. Gardiner, and P. Zoller, Phys. Rev. Lett. **81**, 3108 (1998).
- [15] D. van Oosten, P. van der Straten, and H. T. C. Stoof, Phys. Rev. A **63**, 053601 (2001).
- [16] R. Roth and K. Burnett, Phys. Rev. A **67**, 031602 (2003).
- [17] D. van Oosten, P. van der Straten, and H. T. C. Stoof, Phys. Rev. A **67**, 033606 (2003).
- [18] D. Dickerscheid, D. van Oosten, P. Denteneer, and H. Stoof, Phys. Rev. A **68**, 043623 (2003).
- [19] M. Greiner, O. Mandel, T. Esslinger, T. W. Hänsch, and I. Bloch, Nature **415**, 39 (2002).
- [20] Y. B. Ovchinnikov, J. H. Müller, M. R. Doery, E. J. D. Vredenbregt, K. Helmerson, S. L. Rolston, and W. D. Phillips, Phys. Rev. Lett. **83**, 284 (1999).
- [21] C. Orzel, A. K. Tuchman, M. L. Fenselau, M. Yasuda, and M. A. Kasevich, Science **291**, 2386 (2001).
- [22] M. Greiner, O. Mandel, T. W. Hänsch, and I. Bloch, Nature **419**, 51 (2002).
- [23] F. S. Cataliotti, S. Burger, C. Fort, P. Maddaloni, F. Minardi, A. Trombettoni, A. Smerzi, and M. Inguscio, Science **293**, 843 (2001).
- [24] S. Burger, F. S. Cataliotti, C. Fort, F. Minardi, M. Inguscio, M. L. Chiofalo, and M. P. Tosi, Phys. Rev. Lett. **86**, 4447 (2001).
- [25] O. Morsch, J. H. Müller, M. Cristiani, D. Ciampini, and E. Arimondo, Phys. Rev. Lett. **87**, 140402 (2001).
- [26] M. Cristiani, O. Morsch, J. H. Müller, D. Ciampini, and E. Arimondo, Phys. Rev. A **65**, 063612 (2002).
- [27] A. Trombettoni and A. Smerzi, Phys. Rev. Lett. **86**, 2353 (2001).
- [28] B. Wu and Q. Niu, Phys. Rev. A **64**, 061603 (2001).

- [29] V. V. Konotop and M. Salerno, Phys. Rev. A **65**, 021602 (2002).
- [30] B. B. Baizakov, V. V. Konotop, and M. Salerno, J. Phys. B **35**, 5105 (2002).
- [31] M. Krämer, L. Pitaevskii, and S. Stringari, Phys. Rev. Lett. **88**, 180404 (2002).
- [32] M. Machholm, C. J. Pethick, and H. Smith, Phys. Rev. A **67**, 053613 (2003).
- [33] P. Massignan and M. Modugno, Phys. Rev. A **67**, 023614 (2003).
- [34] J.-P. Martikainen and H. T. C. Stoof, Phys. Rev. Lett. **91**, 240403 (2003).
- [35] E. Cornell, private communication.
- [36] V. Bretin, P. Rosenbusch, F. Chevy, G. V. Shlyapnikov, and J. Dalibard, Phys. Rev. Lett. **90**, 100403 (2003).
- [37] T. Mizushima, M. Ichioka, and K. Machida, Phys. Rev. Lett. **90**, 180401 (2003).
- [38] M. O. Scully and M. S. Zubairy, *Quantum Optics* (Cambridge University Press, Cambridge, 1997).
- [39] J.-P. Martikainen and H. T. C. Stoof (2003), cond-mat/0311382.
- [40] T. Stöferle, H. Moritz, C. Schori, M. Köhl, and T. Esslinger (2003), cond-mat/0312440.
- [41] J.-P. Martikainen and H. T. C. Stoof, Phys. Rev. A **68**, 013610 (2003).
- [42] A. Fetter, Phys. Rev. **162**, 143 (1967).
- [43] J. Javanainen and M. Mackie, Phys. Rev. A **59**, R3186 (1999).
- [44] E. Timmermans, P. Tommasini, R. Côté, M. Hussein, and A. Kerman, Phys. Rev. Lett. **83**, 2691 (1999).
- [45] M. Holland, J. Park, and R. Walser, Phys. Rev. Lett. **86**, 1915 (2001).
- [46] R. Duine and H. T. C. Stoof, J. Opt. B: Quantum Semiclass. Opt. **5**, S212 (2003).
- [47] R. Duine and H. Stoof, submitted to Phys. Rep., cond-mat/0312254.
- [48] K. W. Madison, F. Chevy, V. Bretin, and J. Dalibard, Phys. Rev. Lett. **86**, 4443 (2001).
- [49] B. P. Anderson, P. C. Haljan, C. A. Regal, D. L. Feder, L. A. Collins, C. W. Clark, and E. A. Cornell, Phys. Rev. Lett. **86**, 2926 (2001).
- [50] Y. Castin and R. Dum, Phys. Rev. Lett. **77**, 5315 (1996).
- [51] Y. Kagan, E. L. Surkov, and G. V. Shlyapnikov, Phys. Rev. A **54**, R1753 (1996).
- [52] E. Lundh, C. J. Pethick, and H. Smith, Phys. Rev. A **58**, 4816 (1998).

This figure "Fig6.jpg" is available in "jpg" format from:

<http://arxiv.org/ps/cond-mat/0402052v1>